Engineered Science

RESEARCH PAPER View Article Online

In Situ Preparation of WO_3/g-C_3N_4 Composite and Its Enhanced Photocatalytic Ability, a Comparative Study on the Preparation Methods of Chemical Composite and Mechanical Mixing

Zengying Zhao,[1*] Hua Ma,[1] Mingchao Feng,[1] Zhaohui Li,[2,3] Dapeng Cao[4,5] and Zhanhu Guo[6]

A facile and efficient WO_3/g-C_3N_4 composite photocatalyst was developed by an *in situ* raw material decomposition method. The photocatalyst was synthesized by direct heating low-cost ammonium tungstate and melamine together at the same time. The characterization and photocatalytic performance of the WO_3/g-C_3N_4 chemical composite samples were compared with those from mechanical mixing. The characterization includes X-ray diffraction (XRD), transmission electron microscopy (TEM), X-ray photoelectron spectroscopy (XPS), UV-vis diffuse reflectance spectroscopy (DRS), Fourier transform infrared spectra (FT-IR), etc. The composite formed by the chemical method exhibited obviously better photocatalytic activity than the mechanical mixing sample under visible light irradiation. The possible mechanism for the enhanced catalytic efficiency may be due to the synergistic effect between the WO_3 and g-C_3N_4 tighter interface and the improved optical absorption in visible region.

Keywords: WO_3; g-C_3N_4; Photocatalysis; Comparative study; Chemical composite

Received 3 November 2018**, Accepted** 29 January 2019

DOI: 10.30919/es8d689

1. Introduction

With the fast development of industry, environmental problems have become a severe threat to human beings. As photocatalyst can be applied to wastewater treatment, environmental cleaning, and producing hydrogen from water splitting, etc., it has been attracting much attention in recent years.[1-3] TiO_2 is the most widely used photocatalyst because of its excellent oxidation ability, availability, and stability.[4] However, TiO_2 has low quantum efficiency and it is inactive under visible-light irradiation. Many scientists have tried their best to improve its visible-light response, such as doping with impurity,[5,6] co-catalyst loading,[7] and shape control.[8-9] Scientists have also found other photocatalysts that show high catalytic activity under visible light irradiation. [10] Unfortunately, these types of catalysts, such as $BiVO_4$ and CdS,[11-14] are always toxic for human health and harmful to the environment. As a consequence, it is very important to find new and nontoxic photocatalysts with excellent catalytic activity under visible light.

The stable metal-free photocatalyst, polymeric graphite-like carbon nitride (g-C_3N_4), has attracted great interests recently. It has applications in water splitting and decomposition of organic pollutants under visible light.[15-16] However, the photocatalytic efficiency of the pure g-C_3N_4 is limited by the high recombination rate of its photogenerated electron-hole pairs.[17] One of the techniques for increasing the separation efficiency of photo-generated electron-hole pairs is to form a composite photocatalyst using two kinds of semiconductors.[18] As for g-C_3N_4, various semiconductors composited with g-C_3N_4 have been reported. These semiconductors include TiO_2 [19], ZnO[20], Ag_3PO_4 [21], and Bi_2WO_6 [22], etc. Tungsten oxide (WO_3) is an n-type semiconductor. It has attracted much interest for the uses in electrochromic devices[23], gas sensors[24], and in supercapacitors [25] due to its relatively narrow band gap (i.e. 2.36-2.8 eV) and stable chemical and physical properties. Moreover, WO_3 has also gained much attention as a promising visible light driven photocatalyst in recent years.[30-34] However, pure WO_3 is not an efficient photocatalyst because of its low conduction band (CB) level, which limits its photocatalytic ability to react with electron acceptors such as oxygen.[35]

Although there have been reports of WO_3/g-C_3N_4 photocatalysts, the preparation methods are mechanical mixing of WO_3 and g-C_3N_4,[36-41] and none of these has been focused on the comparative study of samples prepared by *in situ* raw material decomposition and mechanical mixing. In this study, the WO_3/g-C_3N_4 chemical composite photocatalyst has been prepared by an *in situ* decomposition reaction of ammonium tungstate and melamine. Its characterization, the photocatalytic activity

[1]*School of Science, China University of Geosciences, 29 Xueyuan Rd, Beijing 100083, China*
[2]*Beijing Key Laboratory of Materials Utilization of Nonmetallic Minerals and Solid Wastes, National Laboratory of Mineral Materials, School of Materials Science and Technology, China University of Geosciences, Beijing 100083, China*
[3]*Department of Geosciences, University of Wisconsin - Parkside, Kenosha, WI 53141-2000, USA*
[4]*State Key Lab of Organic-Inorganic Composites, Beijing University of Chemical Technology, Beijing 100029, China*
[5]*International Research Center of Soft Matter, Beijing University of Chemical Technology, Beijing 100029, China*
[6]*Integrated Composites Laboratory (ICL), Chemical and Biomolecular Engineering Department, University of Tennessee, Knoxville, TN 37996, USA*
***E-mail:** zhaozy@cugb.edu.cn*

and reaction mechanism in the degradation of methylene blue (MB), have been comparatively discussed with the WO_3/g-C_3N_4 samples created by mechanical mixing.

2. Experimental

2.1 Preparation of photocatalysts

All starting reagents (analytical grade) were purchased from Sinopharm company and were used without further purification. Distilled water was used throughout. Before the reaction, different ratios of ammonium tungstate hydrate and melamine powders were added into a motor and ground for 30 min using a pestle. The resultant mixed powder was added into a crucible with a cover in a semiclosed system. Then it was heated at a heating rate of 20 °C min^{-1} under air conditions. According to thermogravimetric analysis (TG) results (as shown in Fig. S1), the mass contents of WO_3 in the WO_3/g-C_3N_4 chemical composite samples were estimated to be 0.39%, 1.35%, 2.83%, 5.01%, 10.02%, respectively. Therefore, the obtained WO_3/g-C_3N_4 chemical composites with different contents of WO_3 were named as 0.3WN, 1WN, 3WN, 5WN, 10WN. The pure WO_3 and pure g-C_3N_4 samples were also prepared using the same process with ammonium tungstate hydrate or melamine as raw materials, respectively. Besides, a mechanically mixed sample was also prepared by mixing the WO_3 and g-C_3N_4 powders, which has the same amount of WO_3 with that of 3WN, and it was named as mechanical mixing sample 3W--N, in order to compare with the chemical composite sample of 3WN.

2.2 Characterization

The crystal phase composition of the samples was obtained by X-ray diffraction (XRD, Rigaku D/max, Rigaku Corporation, Tokyo, Japan) in the 2θ range of 10-80° using Cu-Kα radiation for the X-ray radiation source. The specific surface area, pore size, and pore volume of the samples were evaluated with a surface area analyzer (AutosorbiQ Station-I, Quantachrome Instruments, Florida, US) from N_2 adsorption isotherms using Brunauer-Emmett-Teller (BET) method. The mesopore size distribution and mesopore volume were calculated by desorption isotherms. The elemental composition of the samples was measured by X-ray photoelectron spectroscopy (XPS, Thermo ESCALAB 250xi) with photon energy of 1253.6 eV, and with Mg-Kα radiation as the exciting source. All the binding energies were referenced to the C1s peak for calibration. The crystal size and morphology of the samples were obtained by scanning electron microscopy (SEM, S-500, JEOL Ltd., Tokyo, Japan) and transmission electron microscopy (TEM, JEM-2100F, JEOL Ltd., Tokyo, Japan). The crystalline structure of the samples was examined by high resolution transmission electron microscopy (HRTEM). The UV-vis absorption spectra of the samples were recorded on a UV-vis scanning spectrophotometer (Perkin-Elmer, Lambda 900, Florida) in the scan range from 200 to 800 nm equipped with an integrated sphere with Barium sulphate ($BaSO_4$) as the reference. The EIS and PT are both tested on an electrochemical workstation (SI 1287, METEK, Benelux, UK) with electrolyte of 0.1M Na_2SO_4 and visible light irradiation of a 500 W Xenon lamp.

2.3 Photoreaction apparatus and procedure

Photocatalytic activities of WO_3/g-C_3N_4 chemical composite samples were evaluated by degradation of MB (2×10^{-5} mol/L) under visible light irradiation of a 500 W Xenon lamp with 420 nm cutoff filters. In a typical procedure, 50 mg of photocatalyst was dispersed into 50 mL of MB solution. Before illumination, the photocatalyst powder and dye solution were stirred in dark for 60 min to achieve the adsorption-desorption equilibrium of suspensions. Afterward, about 3 mL of the reaction solution was taken at given time intervals, and separated through centrifugation. The concentration of MB was analyzed by recording the absorbance at the characteristic band of 664 nm by a U-3010 UV-vis spectrophotometer.

3. Results and discussion

3.1 XRD analysis

Fig.1 shows the XRD patterns of the WO_3, g-C_3N_4, chemical composite samples 0.3WN, 1WN, 3WN, and 5WN, and mechanical mixing sample 3W--N. The XRD pattern of the WO_3 can be exactly indexed as the monoclinic structure (JCPDS 43-1035).[18] For pure g-C_3N_4, the strongest XRD peak at 27.30°, corresponding to 0.326 nm, can be indexed as (002) diffraction plane (JCPDS 87-1526). It is due to the stacking of the conjugated aromatic system as in graphite. Another pronounced additional peak is found at 12.80°, corresponding to a distance of 0.675 nm. This distance is only slightly below the size of one tris-s-triazine unit (ca. 0.73 nm). The two diffraction peaks are in good agreement with the reported results of g-C_3N_4.[41] For the

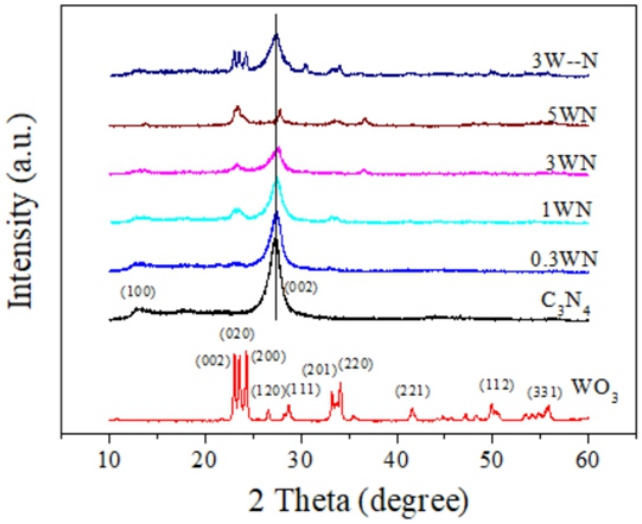

Fig. 1 XRD patterns of WO_3, g-C_3N_4, WO_3/g-C_3N_4 chemical composite samples and mechanical mixing sample.

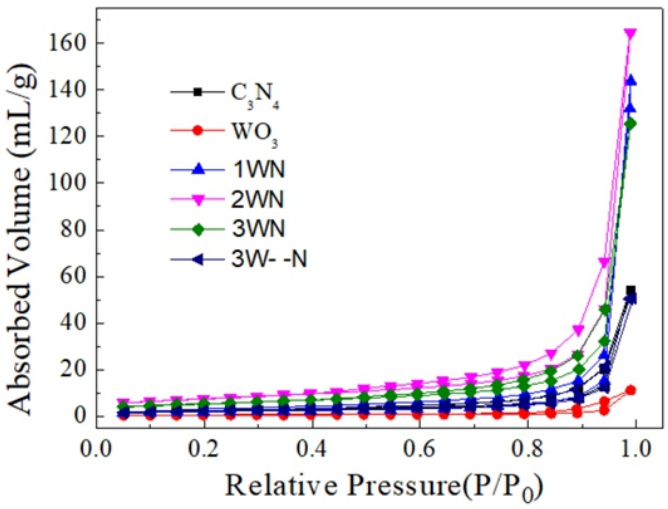

Fig. 2 N_2 adsorption-desorption isotherms of the chemical composite samples and the mechanical mixing sample 3W--N.

mechanical mixing sample 3W--N, the XRD patterns reveal a coexistence of WO_3 and g-C_3N_4 with the appearance of three WO_3 typical peaks: (002), (020) and (200) and two g-C_3N_4 peaks: (100) and (002). On the contrary, in the chemical composite sample 3WN, the three peaks have combined to a broad peak. It may that the (as also shown in the following TEM images). Moreover, the intensity of the above-mentioned WO_3 broad peak increases gradually with the increasing of the WO_3 content in the samples; and it is also interesting to note that the peak of g-C_3N_4 decreased at the same time.

Besides, it is observed that in the chemical composite samples, the (002) peak of g-C_3N_4 shifted from 27.30° to 27.77°. Based on this result, it is proposed that the coupling between WO_3 and g-C_3N_4 may happen on the g-C_3N_4 (002) facet.[42] By contrast, from Fig. 1, there are no shifts of the diffraction peaks in the mixed sample 3W--N. This proved that there is no tight interaction between the WO_3 and C_3N_4 in the mechanical mixing sample 3W--N.

3.2 BET Test

BET N_2-sorption measurements can be used to investigate the surface areas, pore volumes, and average pore diameters of the samples. The recorded N_2 adsorption-desorption isotherms for the chemical composite sample and the mechanical mixing sample are shown in Fig. 2. The N_2 adsorption-desorption isotherm include six types from I to VI, indicating the existence of micropore solids, non-hole or macropore structure, the interaction of gas-solid on non-hole or macropore materials, mesoporous structure, the interaction of gas-solid on micropore and mesoporous materials, and the multilayer adsorption on surface of nonhole materials, respectively. The isotherm of all the samples are type II. And both of them are with H3 hysteresis loop, indicating the existence of non-hole or macropore structure according to the IUPAC classification.[43-44]

According to the BET measured results, the specific surface areas, pore sizes and pore volumes of the samples were calculated, and the results are listed in Table 1. The samples show obvious difference in their surface areas, which are 7.323 and 18.984 m^2g^{-1}, for the mechanical mixing sample 3W--N and the chemical composite sample 3WN, respectively. The specific surface area of the chemical composite 3WN is much higher than that of the mechanical mixing 3W--N. This is perhaps because that the g-C_3N_4 has become more porous in its preparation from the raw material of ammonium tungstate hydrate and melamine. The larger specific surface area of 3WN can provide abundant reacting active sites for the reactive molecules to contact with the photocatalyst, thus improving its photocatalytic performance.

3.3 SEM, TEM and HRTEM analyses

Fig. 3 shows the SEM images of the chemical composite sample 3WN and mechanical mixing sample 3W--N. The chemical composite sample has an uneven surface (Fig. 3a), which indicates that the surface of g-C_3N_4 in the composite sample has been etched by the thermal treatment in the preparation procedure. Furthermore, the uneven sheets of g-C_3N_4 covered the WO_3 particles in the 3WN sample, while the g-C_3N_4 and the WO_3 particles are departed from each other.

TEM and HR-TEM can be used to investigate the morphology and microstructure of the samples. Fig. 4(a and b) shows the TEM and HRTEM images of the mechanical mixing sample 3W--N. It can be seen that the WO_3 are uneven grainy particles with particle size about 1 um; while the C_3N_4 are thin sheets, and there have clear boundaries between the WO_3 and C_3N_4 parts in the sample. As for the chemical composite sample 3WN as showed in Fig. 4(c and d), it is obvious different from the mechanical mixing sample. Its WO_3 parts are nanorods with width about 10 nm and different lengths from 80 to 100 nm. There are no clear boundaries between the WO_3 and g-C_3N_4 parts,

Table 1 Structural properties of the mechanical mixing sample 3W--N and chemical composite sample 3WN.

Sample	S_{BET} [a] (m^2 g^{-1})	PV [b] (cm^3)	PD[c] (nm)
3W--N	7.323	0.059	3.785
3WN	18.984	0.032	4.396

a: the specific surface area was calculated using BET equation; b: pore volume; c: pore diameter.

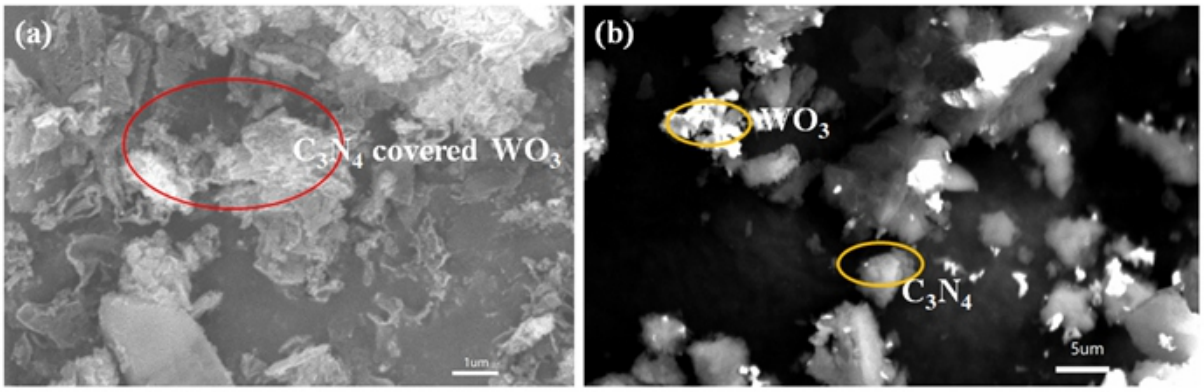

Fig. 3 (a) SEM images of chemical composite sample 3WN and (b) mechanical mixing sample 3W--N.

for the two parts look like fused together without any apparent dividing lines. Another main difference from sample 3W--N is that the WO_3 rods are wrapped by corrugated and almost transparent g-C_3N_4 sheets in the chemical composite sample 3WN.

3.4 XPS analysis

X-ray photoelectron spectroscopy (XPS) can further confirm the local structure of WO_3 and g-C_3N_4 in the materials. Fig. 5(a) shows the survey scan XPS spectra of mechanical mixing sample 3W--N and chemical composite sample 3WN. The result indicates the presence of W, O, C, and N elements in both the samples and there are no obvious differences between the two samples. High resolution spectra of C1s, N1s, O1s, and W4f of the sample 3WN are shown in Fig. 5(b-e). The C1s in 3WN has two peaks at 284.4 and 288.0 eV, respectively. The former is assigned to the adventitious carbon on the surface of composite sample 3WN. The other C1s peak at 288.0 eV is attributed to

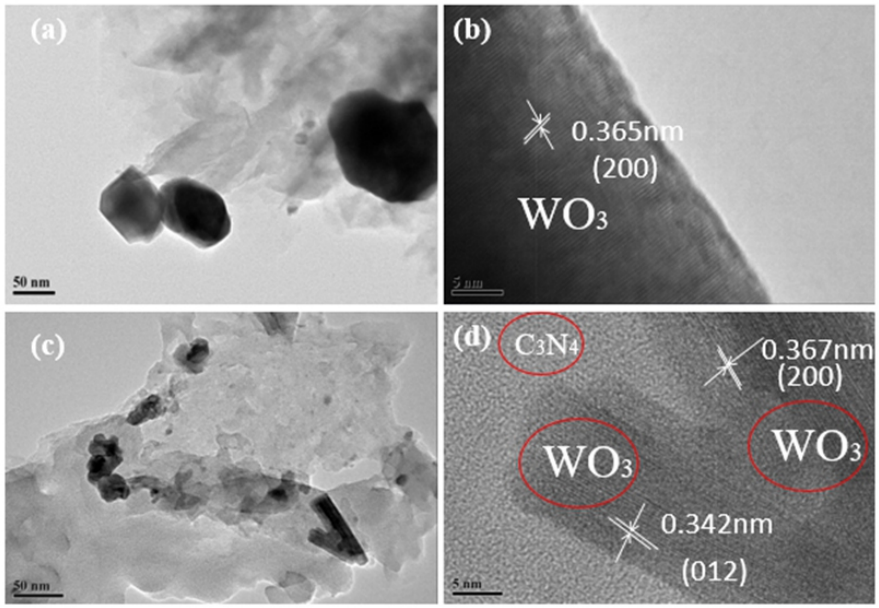

Fig. 4 TEM and HRTEM of mechanical mixing sample 3W--N (a and b) and chemical composite sample 3WN (c and d).

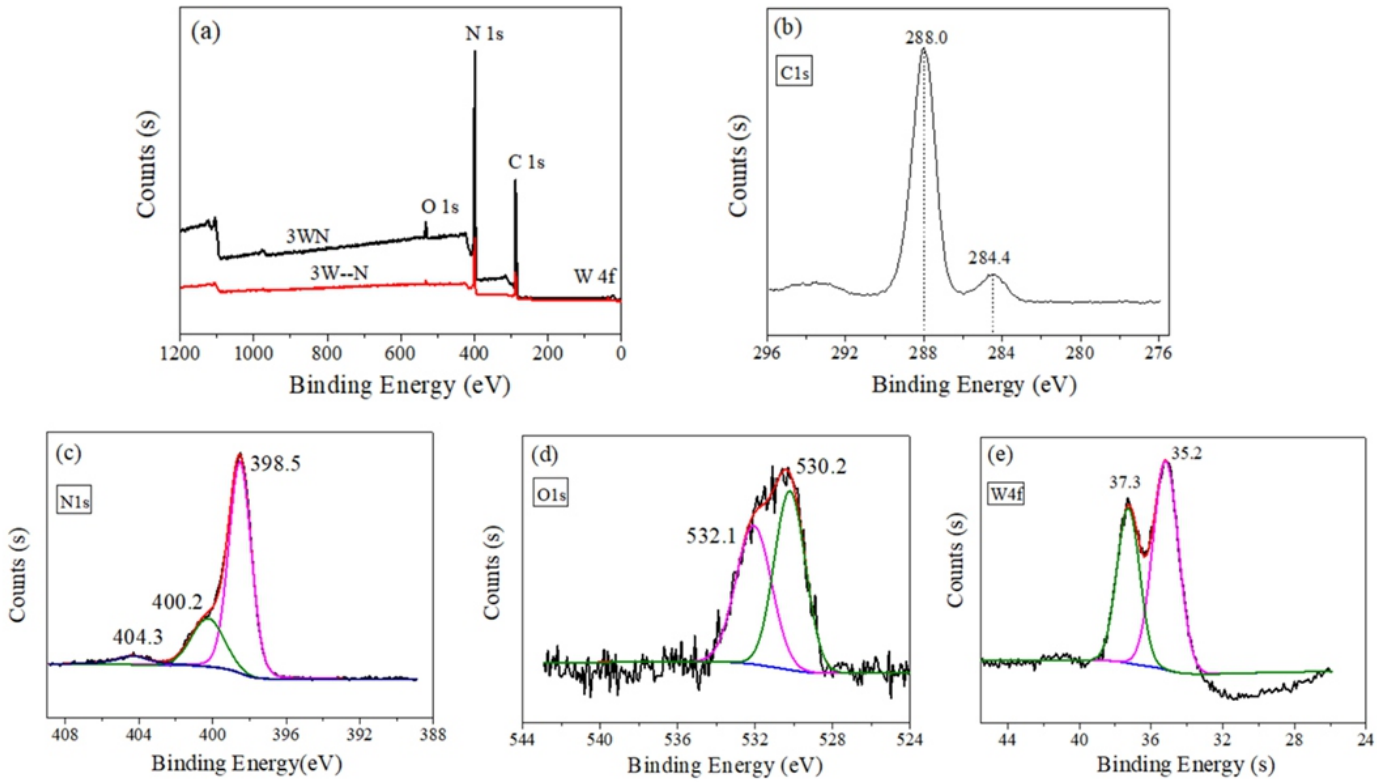

Fig. 5 (a) XPS survey spectra of mechanical mixing sample 3W--N and chemical composite sample 3WN, (b-e) high resolution XPS spectra of C1s, N1s, O1s, and W4f.

a C-N-C coordination in g-C_3N_4.[45] The N1s spectrum can be separated to several binding energy peaks. The main N1s peak at a binding energy of 398.5 eV can be assigned to sp^2-hybridized nitrogen (C=N–C), which confirms the presence of sp^2-bonded graphitic carbon nitride. The peaks at 400.2 eV is attributed to tertiary nitrogen groups N–$(C)_3$, and the peaks at 404.3 eV is assigned to the terminal amino-group at the g-C_3N_4 molecule. The O1s peak centred at 530.2 eV is associated with the O2- in the WO_3. The other O1s peak at 532.1 eV is associated with an -OH group or water molecule on the surface of the composite sample.[46-47] The binding energy values of W4f7/2 and W4f5/2 are observed at 35.2 eV and 37.3 eV, respectively, which are consistent with the XPS results provided by the literatures reported for WO_3.[48-49] All the above data is similar with those of the mechanical mixing sample 3W--N as showed in supplemental Fig. S3. This indicated that there have no chemical interaction between the WO_3 and g-C_3N_4 parts in the chemical composite samples.

3.5 FT-IR and DRS analysis

Fig. 6 shows the FT-IR spectra of the as synthesized mechanical mixing sample 3W--N and chemical composite samples 1WN and 3WN. For both samples, several bands in the 1200-1650 cm^{-1} region were found, which correspond to the typical stretching modes of CN heterocycles. The sharp band at 810 cm^{-1} and the broad bands at around 3000 cm^{-1} are indicative of the triazine units and the NH stretching vibration modes, respectively .[40] While the chemical composite sample 3WN has a relatively higher transmission and weaker absorption at 1200-1650 cm^{-1} and 810 cm^{-1}, which may result from the different concentration of the composite during the experiment. Therefore, it exists mainly a physical interaction between g-C_3N_4 and WO_3 in both chemical composite sample and mechanical mixing sample.

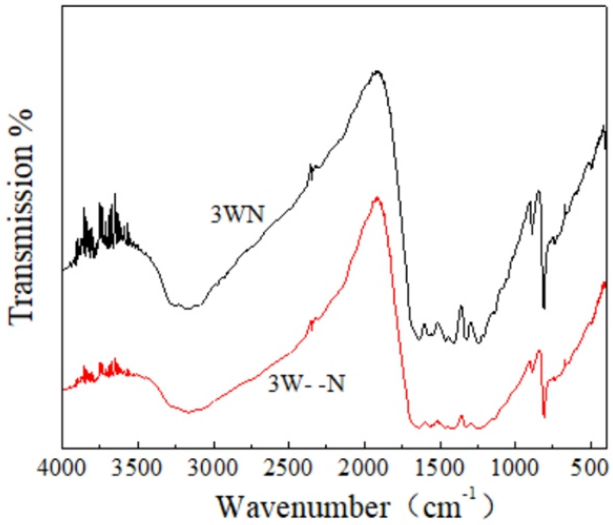

Fig. 6 FT-IR spectra for the g-C_3N_4, WO_3, mechanical mixing sample 3W--N and chemical composite samples 1WN and 3WN.

The optical properties of the g-C_3N_4, WO_3, mechanical mixing sample 3W--N and chemical composite sample 3WN were examined by UV-vis diffuse reflectance spectroscopy. For all samples, the optical absorption edge was estimated to be at around 480 nm (Fig. 7). The g-C_3N_4 sample shows absorption wavelengths from UV to visible region ranging up to 460 nm. Compared with pure g-C_3N_4, the spectrums of composite samples are shifted to longer wavelengths. Obvious enhanced absorption in the visible region is also observed. Moreover, the red shift and the light absorbance are strengthened with the increase of the WO_3 amount in the chemical composite samples, which subsequently results in the efficient utilization of visible light. The absorbance to the visible light can also be enhanced by the adding of WO_3 in the mechanical mixing sample 3W--N. However, if the amount of WO_3 is the same in the samples, the chemical composite sample 3WN has better light absorption than the mechanical mixing sample. From the UV-vis results, it can be concluded that the chemical composite sample 3WN should generate more electron-hole pairs under visible light irradiation, and exhibit high photocatalytic activity. It is supposed that the reason is the tight interaction between the g-C_3N_4 and WO_3 parts in the sample, in addition to the high crystallinity of the WO_3 in the chemical composite sample due to the calcination procedure during the sample preparation. This high crystallinity can be seen when compared with the mechanical mixing sample 3W--N as shown in the TEM (Fig. 4).

3.6 Evaluation of photocatalytic activity

In order to investigate the photocatalytic activity of the as prepared photocatalyst samples, the relationship between the photooxidation efficiency of MB and the illumination time for different photocatalysts are shown in Fig. 8. It can be seen that the degradation efficiencies of

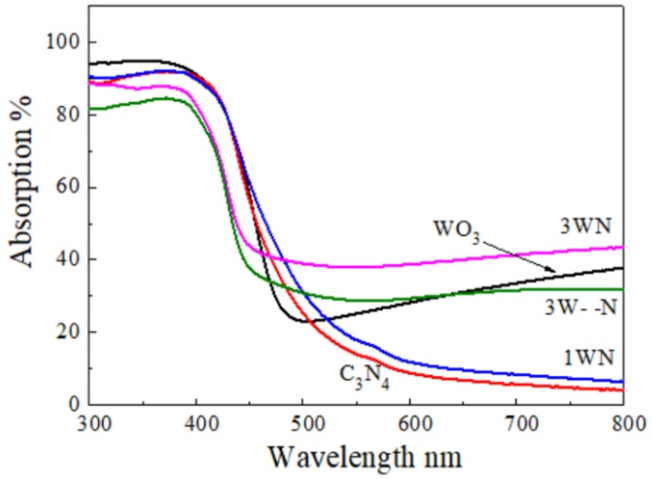

Fig. 7 Typical UV-vis spectra of g-C_3N_4, WO_3, mechanical mixing sample 3W--N and chemical composite sample 3WN.

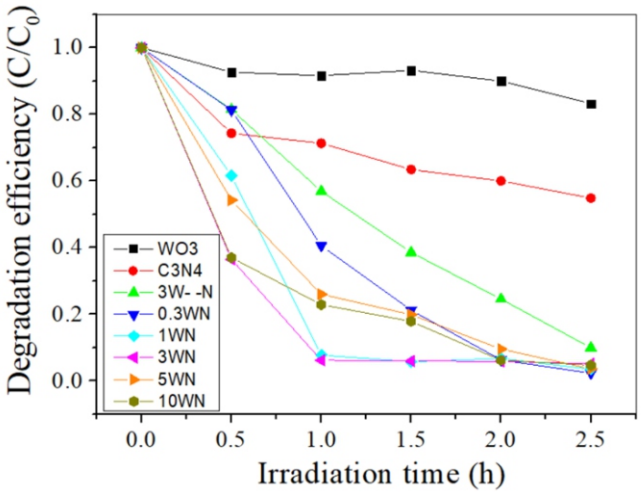

Fig. 8 Photocatalytic degradation efficiency of MB by g-C_3N_4, WO_3, mechanical mixing and chemical composite samples.

MB for the as prepared WO_3 and mechanical mixing sample 3W--N were about 17% and 45% for irradiation time of one hour, respectively. In contrast, there are obvious better degradation efficiencies for the chemical composite catalysts. When the WO_3 content in the composite sample is 3 wt%, it takes one hour to degrade 96% of the MB, which presents the (b) highest efficiency in all the catalyst samples.

3.7 EIS and photocurrent analysis

Electrochemical impedance spectra are obtained to elucidate the transfer and migration processes of the photoexcited e^--h^+ pairs.[50] Fig. 9(a) shows the electrochemical impedance spectra (EIS) of samples under light conditions. We found that the charge transfer resistance of the composite sample 3WN is quite smaller compared with those of all other samples. This proved that the WO_3/g-C_3N_4 chemical composited sample 3WN has the highest efficiency in charge transfer in all the samples. This result is also consistent with the photocatalytic efficiency when using MB as a target organic pollutant as showed in Fig 8. Moreover, Fig. 9(b) shows the charge transfer resistance of chemical composite sample 3WN under light and dark condition, respectively. The result indicates that under the light irradiation, there will be more photo-induced carriers generated compared with in dark condition.

Photocurrent-time (PT) can reveal the interfacial generation and separation dynamics of photogenerated charges of semiconductor photocatalysts, and a larger photocurrent indicates higher electrons and holes separation efficiency[51] Fig.10 shows the PT curves of the samples excited by visible light pulse. It can be seen that the chemical composite 3WN has the largest current response. This indicates that the chemical composite sample 3WN has higher charge separation efficiency than mechanical mixing sample, so the sample 3WN has the best photocatalytic performance. Therefore, the chemical composite preparation method of The chemical composite WO_3/g-C_3N_4 has an advantage over mechanical mixing method.

As discussed above, when a closed interaction between WO_3 and g-C_3N_4 is formed, photoexcited electrons in the CB of WO_3 and photoexcited holes in the VB of g-C_3N_4 can achieve a fast combination as shown by the red arrow in Fig. 11. At the same time, the electrons in the CB of g-C_3N_4, which have more negative potential, and the holes in the VB of WO_3, which have more positive potential, can provide an obvious enhanced photocatalytic activity for the as prepared WO_3/g-C_3N_4 photocatalyst.

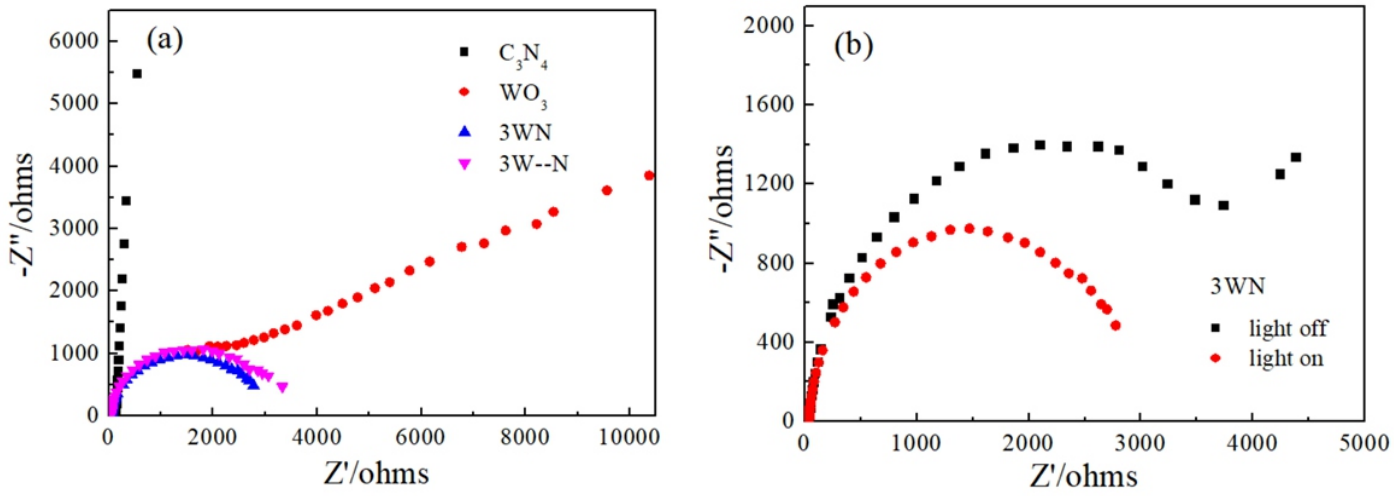

Fig. 9 EIS of C_3N_4, WO_3, 3WN and 3W--N under light conditions (a); EIS of 3WN under light and dark conditions (b).

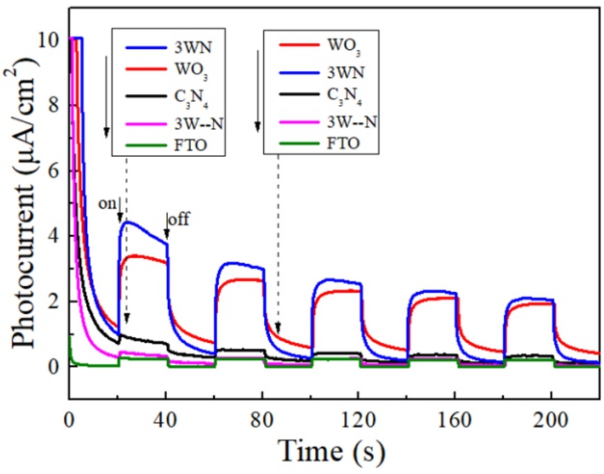

Fig. 10 Transient photocurrent responses of C_3N_4, WO_3, 3WN and 3W--N under visible light irradiation.

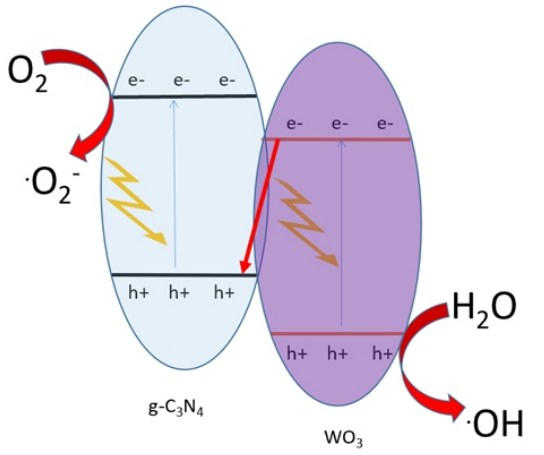

Fig. 11 Schematic diagram of photoexcited electron-hole separation process.

Conclusions

The chemical composite WO_3/g-C_3N_4 has been synthesized successfully by an in situ decomposition of melamine and ammonium tungstate hydrate. And the comparative research was carried out between the chemical composite samples and the mechanical mixing samples in the aspect of microscopic structure, composition, morphology, photocatalytic ability and photocatalytic mechanism. The highest degradation efficiency of MB was achieved by the chemical composite sample, which induced 96% degradation of MB within 1 h under visible light irradiation. While the degradation rate is only 45% by the mechanical mixing sample. The enhanced photocatalytic activity can be attributed to the synergy effect between the tighter interaction of WO_3 and g-C_3N_4 in the chemical composite sample. This result can be understood by the UV-Vis, EIS and PT tests, which shows the higher visible light absorption, higher photogenerated electron-hole pairs transfer and separation efficiency.

Acknowledgments

This work was supported by the Fundamental Research Funds for the Central Universities of China [Grant Nos. 2652017153].

References

1. G. Liu, P. Niu, C.H. Sun, S.C. Smith, Z.G. Chen, G.Q. Lu and H. M. Cheng, *J. Am. Chem. Soc*., 2010, **132**, 11642-11648.
2. Q. Xiang, J.G. Yu and M. Jaroniec, *J. Am. Chem. Soc*., 2012, **143**, 6575-6578.
3. Z. Zhao, B. Zhang and D. Chen, *J. Nanosci. Nanotechnol*., 2015, **15**, 1-6.
4. Z. Jin, N. Murakamia, T. Tsubotaa and T. Ohnoa, *Appl. Catal., B: Environ.,* 2014, **150**, 479- 485.
5. T. Ohno, M. Akiyoshi, T. Umebayashi, K. Asai, T. Mitsui and M. Matsumura, *Appl. Catal., A: General,* 2004, **265**, 15-121.
6. T. Ohno, T. Tsubota, K. Nishijima and Z. Miyamoto, *Chem. Lett.*, 2004, **33**, 750-751.
7. S. Sato and J. White, *J. Am. Chem. Soc*., 1980, **102**, 7206-7210.
8. N. Murakami, Y. Kurihara, T. Tsubota and T. Ohno, *J. Phys. Chem. C,* 2009, **113**, 3062-3069.
9. T. Ohno, K. Sarukawa and M. Matsumura, *New J. Chem.*, 2002, **26**, 1167-1170.
10. Y. Zang, L. Li, Y. Zuo and X. Guana, *RSC Adv.*, 2013, **3**, 13646-13650.
11 K. Sayama, A. Nomura, Z. Zou, R. Abe, Y. Abe and H. Arakawa, *Chem. Commun.,* 2003, **35**, 2908-2909.
12. J. Yu and A. Kudo, *Adv. Funct. Mater.,* 2006, **16**, 2163-2169.
13. J. Jang, U. A. Joshi and J. S. Lee, *J. Phys. Chem. C*, 2007, **111**, 13280-13287.
14. Y. Kim and H. Park, *Energy Environ. Sci.,* 2011, **4**, 685-694.
15. X. Wang, K. Maeda, X. Chen, K. Takanabe, K. Domen, Y. Hou, X. Fu and M. Antonietti, *J. Am. Chem. Soc.*, 2009, **131**, 1680-1681.
16. J. Jiang, J. Yu and S. Cao, *J. Colloid Interface Sci*., 2016, **461**, 56-63.
17. S. Yan, Z. Li and Z. Zou, *Langmuir*, 2009, **25**, 10397-10401.
18. H. Katsumata, Y. Tachi, T. Suzuki and S. Kaneco, *RSC Adv*., 2014, **4**, 21405-21409.
19. X. Lu, Q. Wang and D. Cui, *J. Mater. Sci. Technol.*, 2010, **26**, 925-928.
20. Y. Wang, R. Shi, J. Lin and Y. Zhu, *Energy Environ. Sci*., 2011, **4**, 2922-2927.
21. S. Kumar, T. Surendar, A. Baruah and V. Shanker, *J. Mater. Chem. A,* 2013, **10**, 5333-5338.
22. L. Ge, C. Han and J. Liu, *Appl. Catal., B,* 2011, **100**, 108-109.
23. D. Ma, H. Wang, Q. Zhang and Y. Li, *J. Mater. Chem*., 2012, **22**, 16633-16639.
24. S. Vallejos, T. Stoycheva, P. Umek, C. Navio, R. Snyders, C. Bittencourt, E. Llobet, C. Blackman, S. Moniz and X. Correig, *Chem. Commun.*, 2011, **47**, 565-567.
25. X. Lu, T. Zhai, X. Zhang, Y. Shen, L. Yuan, B. Hu, L. Gong, J. Chen, Y. Gao, J. Zhou, Y. Tong and Z. Wang, *Adv. Mater.*, 2012, **24**, 938-944.
26. X. An, J. Yu, Y. Wang, Y. Hu, X. Yu and G. Zhang, *J. Mater. Chem*., 2012, **22**, 8525-8531.
27. P. Chen, P. Xing, Z. Chen, X. Hu, H. Lin, L. Zhao and Y. He, *J. Colloid Interface Sci.*, 2019, 534, 163-171.
28. J. Yu, Z. Chen, Y. Wang, Y. Ma, Z. Feng, H. Lin, Y. Wu, L. Zhao and Y. He, *J. Mater. Sci.,* 2018, 53, 7453-7465.
29. Z. Feng, L. Zeng, Y. Chen, Y. Ma, C. Zhao, R. Jin, Y. Lu, Y. Wu and Y. He, *J. Mater. Res.,* 2017, 32, 3660-3668.
30. G. Xi, J. Ye, Q. Ma, N. Su, H. Bai and C. Wang, *J. Am. Chem. Soc.*, 2012, **134**, 6508-6511.
31. J. Su, L. Guo, N. Bao and C. Grimes, *Nano Lett*., 2011, **11**, 1928-1933.
32. F. Wang, Y. Wang, X. Zhan, M. Safdar, J. Gong and J. He, *Cryst. Eng. Comm.*, 2014, **16**, 1389-1385.
33. J. Yu, Q. Nong, X. Jiang, X. Liu, Y. Wu and Y. He, *Sol. Energy,* 2016, 139, 355-364.
34. Y. He, Li. Zhang, M. Fan, X. Wang, M. Walbridge, Q. Nong, Y. Wu and L. Zhao, *Sol. Energy. Mat. Sol. C*, 2015, 137, 175-184.
35. M. Miyauchi, *Phys. Chem. Chem. Phys*., 2008, **10**, 6258-6266.
36. R. Abe, *Bull. Chem. Soc. Jpn*., 2011, **84**, 1000-1030.
37. A. Doan, X.Thi, P. Nguyen, V. Thi, S. Kim and V. Vo, *Korean Chem. Soc*., 2014, **35**, 6-15.
38. Z. Jin, N. Murakami, T. Tsubota and T. Ohno, *Appl. Catal., B: Environ.* 2014, **150**, 479-485.
39. M. Yang, S. Hua, F. Lia, Z. Fan, F. Wang, D. Liu and J. Gui, *Photocataly. Ceram. Int*., 2014 , **40**, 11963-11969.
40. K. Katsumat, R. Motoyoshi, N. Matsushita and K. Okada, *J. Hazard. Mater.*, 2013, **260**, 475- 482.
41. K. Maeda, X. Wang, Y. Nishihara, D. Lu, M. Antonietti and K. Domen, *J. Phys. Chem. C*, 2009, **113**, 4940-4947.
42. L. Ye, J. Liu, Z. Jiang, T. Peng and L. Zan, *Appl. Catal., B: Environ.*, 2013, **143**, 1-7.
43. L. Hua, H. Xu, Y. Li, H. Li, X. Cheng, J. Xia, Y. Xu and G. Cai, *Dalton Trans.*, 2013, **42**, 8606-8612.
44. J. Xie, L. Bian, L. Yao, Y. J. Hao and Y. Wei, *Mater. Lett.*, 2013, **91**, 213-216.
45. S. Talapaneni, S. Anandan, G. Mane, C. Anand, D. Dhawale and S. Varghese, *J. Mater. Chem*., 2012, **22**, 9831-9839.
46. A. Chakraborty and M. Kebede and R. Kinet., *Mech. Catal.*, 2012, **106**, 83-98.
47. L. Huang, H. Xu and Y. Li, *Dalton Trans*, 2013, **42**, 8606-8617.
48. G. Lu, X. Li, Z. Qu, Q. Zhao, H. Li, Y. Shen and G. Chen, *Chem. Eng. J.*, 2010, **159**, 242-246.
49. R. Sivakumar, R. Gopalakrishnan, M. Jayachandran and C. Sanjeeviraja, *Smart Mater. Struct.*, 2006, **15**, 877-888.
50. H. Cui , B. Li , Z. Li , X. Li and S. Xu, *Appl. Surf. Sci*., 2018, **30**, 831-840.
51. H. Huang, C. Zeng, K. Xiao and Y. Zhang, *J. Colloid Interface. Sci*., 2017, **504**, 257-267.

